Reaction Dynamics on $^{64}Zn + ^{58}Ni$ at 35A-79A MeV with Antisymmetrized Molecular Dynamics Model

R. Wada, K. Hagel, J. Cibor, J. Li, M. Murray, J. B. Natowitz, A. Ono* and
GANIL E160 collaborators
*Department of Physics, Tohoku University, Sendai, Japan

The reaction mechanism and multifragmentation process in $^{64}Zn + ^{58}Ni$ reactions at 35A-79A MeV have been studied by comparing the experimental results to the calculated results obtained with the Antisymmetric Molecular Dynamics Model (AMD-V) of Ono et al.[1]. A brief report about the experiment was also given in the 1998 annual report.

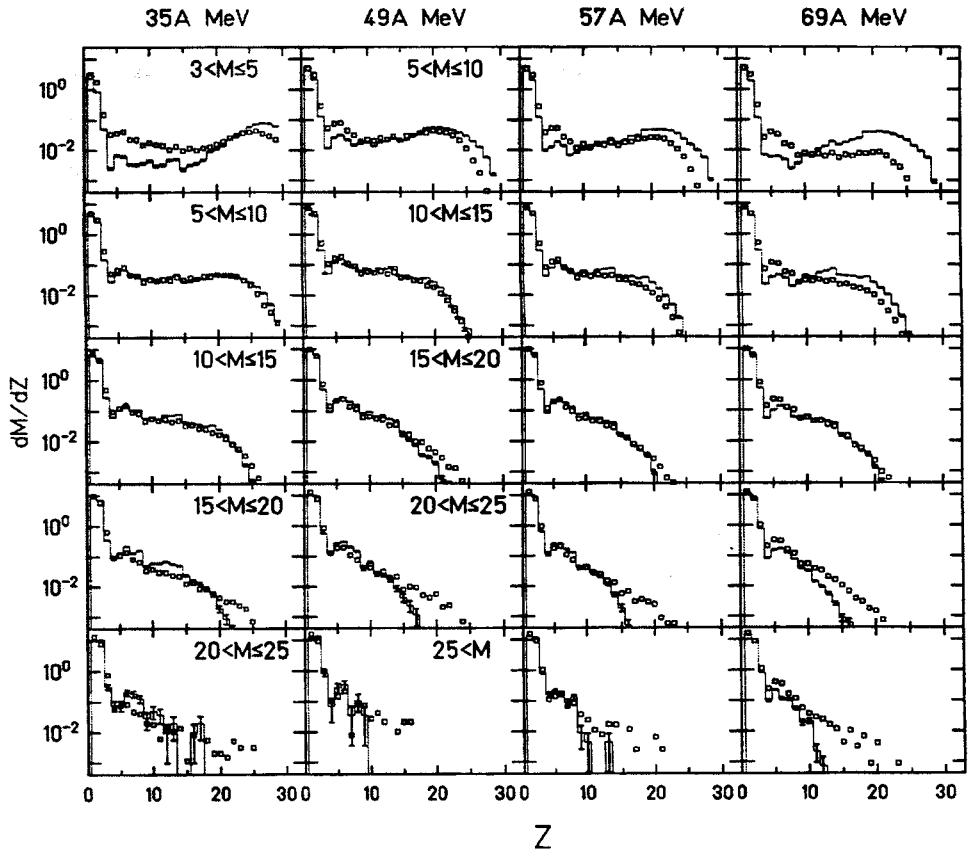

Figure 1. Energy and angle integrated charge distributions for different charged particle multiplicity windows at different incident energies. The incident energy is indicated at the top of each column. The range of the multiplicity window applied is given in the figures for 35A MeV and 49AMeV. Those for the higher incident energies are the same as those for 49A MeV. Experimental results are shown by squares and the calculated results are shown by histograms. Both results are plotted as absolute multiplicity per unit charge. Errors indicate the statistical errors only for the calculated results. Experimental errors are smaller by a factor of 2-3 than those of the calculations at the same multiplicity.

In Fig.1 the experimental charge distributions in the different associated charged particle multiplicity windows are compared with the AMD-V simulations at different incident energies. The charge distributions are obtained by integrating over the observed energy and angular ranges of each fragment. The evolution of the experimental charge distributions for different multiplicity windows is very well reproduced by

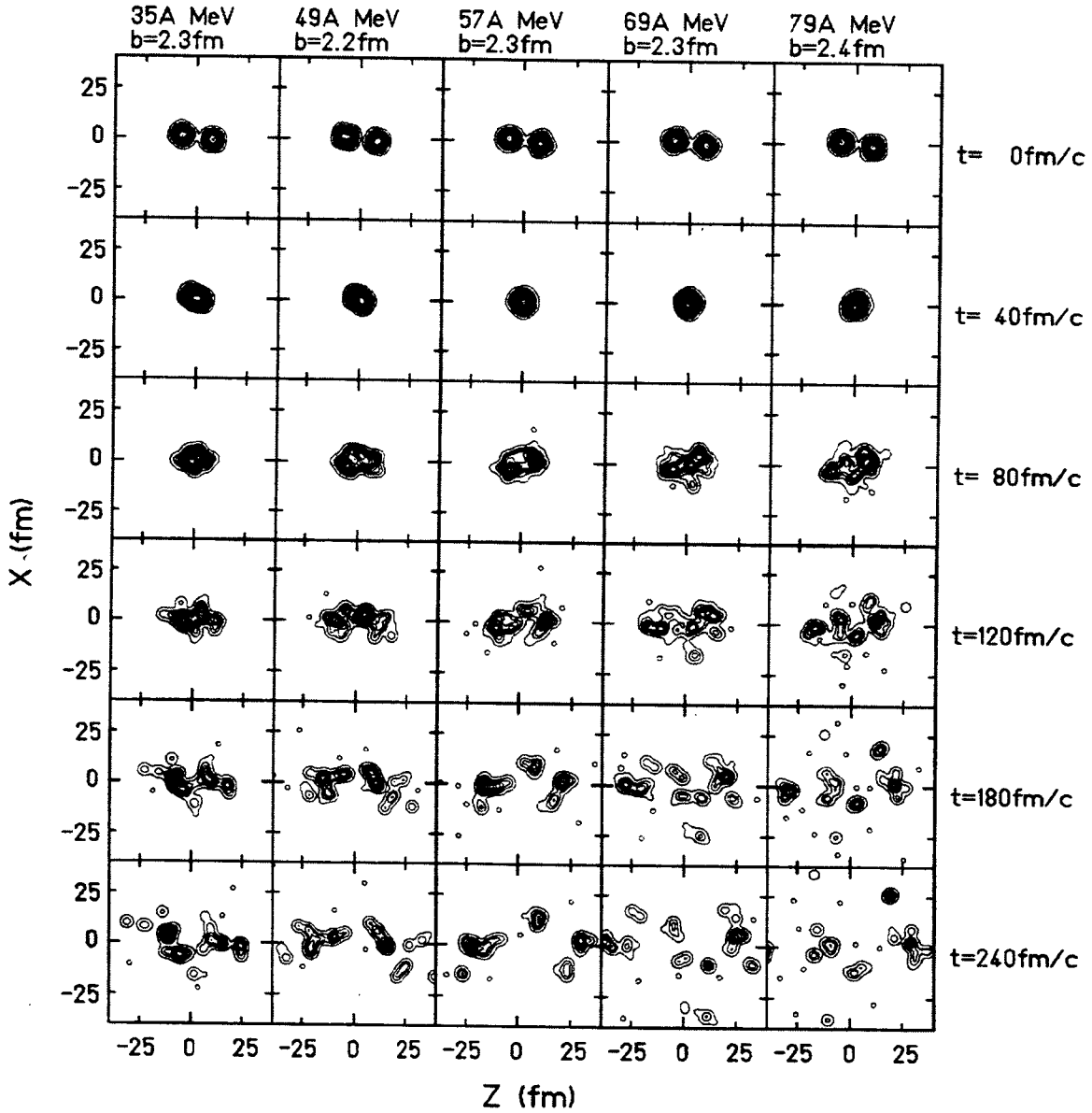

Figure 2. Time evolution of nuclear density distributions, projected on the reaction plane (X-Z plane), for a calculated event with b 2.3fm at different reaction times for all incident energies. Th incident energy is indicated at the top of each column with the impact parameter. The plotted time is indicated on the right. The Z axis is taken as the beam direction and the contour scale is in linear. The smallest circle indicates a nucleon.

the calculations at all incident energies, although there are some discrepancies. For the lowest multiplicity window the experimental distribution is rather poorly reproduced. This is caused by the fact that the approximated density distribution in the physical coordinate space, used for two nucleon collision processes, has a slightly larger radius than that of the exact calculation. Since peripheral collisions are governed by the two nucleon collisions at the nuclear surface, this small deviation in the density distribution affects these events significantly. For the higher multiplicity windows an excess of multiplicity is also generally observed near the largest IMF. This excess appears to be caused by accidental events, where two reactions occur in one beam burst. In such events one of the reactions has to be a violent collision to produce enough associated charged particles and the other is more likely to be a peripheral collision, which has a large cross section and likely has a large fragment. Such events have been largely conservation, in which the sum of the parallel momenta of the observed charged particles is required to be less than the beam momentum. This procedure eliminates most of such events in the lower multiplicity windows, but not completely in the higher multiplicity windows.

In order to elucidate the reaction mechanisms, the simulated AMD-V events have been investigated in detail. In Fig.2 the time evolutions of the nuclear density distributions projected onto the reaction plane are shown for a collision with b $\approx$ 2.3fm at different incident energies. As seen in the figure the projectile and the target merge together around t = 40fm/c at all incident energies and stay as a single system only up to t $\approx$ 120fm/c at 35A MeV and t $\approx$ 80fm/c at 79A MeV. Preequilibrium nucleons appear by 180fm/c at 35A MeV and by t $\approx$ 120fm/c at higher incident energies. The system starts to break into small pieces at t $\approx$ 120fm/c at 35A MeV and at t $\approx$ 80fm/c at 79A MeV. The multifragmentation is a general feature for central or mid-central collisions in this reaction system at these incident energies. In the top row of Fig.3, the average number of nucleons of the projectile or of the target, which cross Z=0, from one side to the other in the center of mass system, is plotted as a function of time. The number is evaluated by averaging over the events with b $\leq$ 3fm and scaled by the number of nucleons in each initial nucleus. For all the cases about 75% of nucleons on average appear on the opposite side. This observation indicates that a certain degree of the nuclear transparency exists. In order to study this transparency further, contour plots of the average nuclear density, projected on the Z axis, versus reaction time are made for central events and shown in the lower part of Fig.3. The initial two ridges merge together at $\approx$ 40-50fm/c, as the projectile and the target overlap. After the two nuclei merge together, the two ridges are still observed similar to those seen in the heavy ion simulations in the TDHF calculations at low incident energies. This transparency, however, is quite different from those of the TDHF calculations. First of all the density of these ridges disappears gradually with the reaction time. This indicates that the projectile and target nuclei break into small pieces and spread widely along the ridges. Secondly the slope of the ridges is significantly steeper than that of the incident nuclei. This indicates that the projectile and target are significantly slowed down during the collisions. In the nucleon transport, the reaction shows a transparency, whereas, in the energy transport, the reaction is not transparent. We, therefore, designate this as semi transparency.

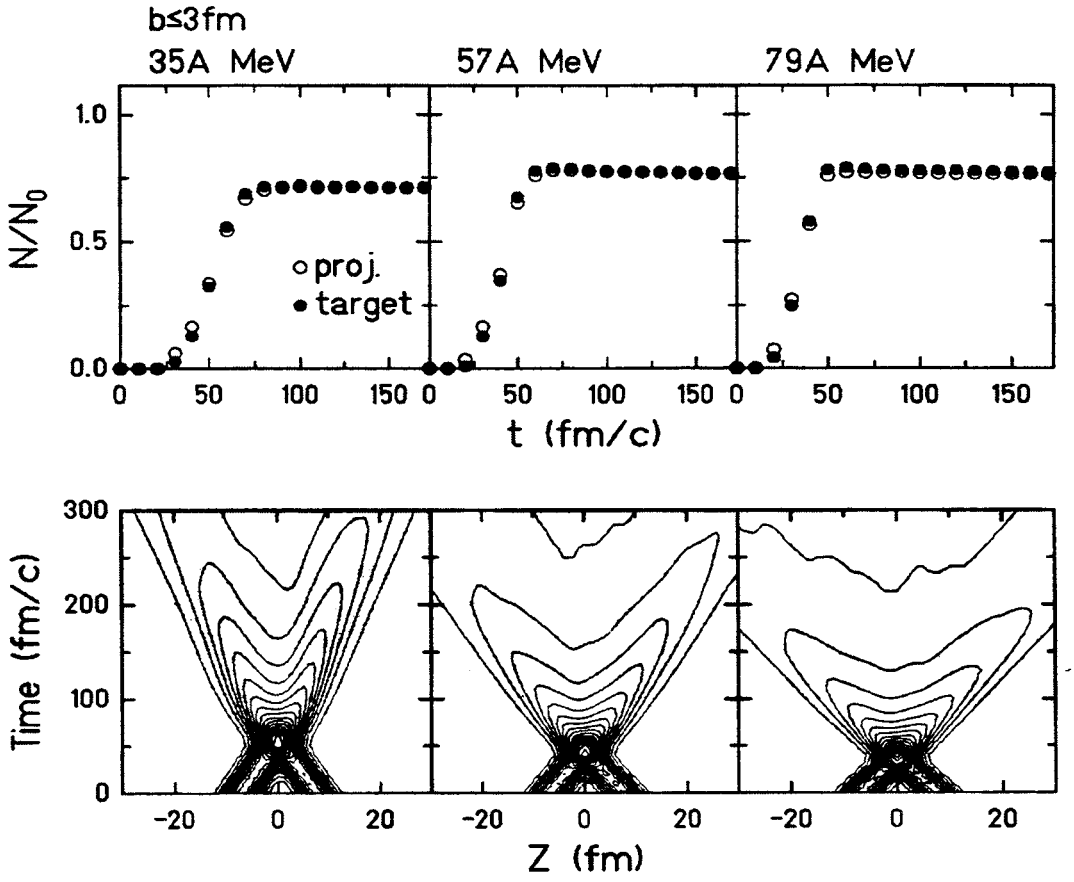

Figure 3. Upper: The average number of nucleons in the initial nuclei across Z=0 from one side to the other is plotted as a function of time for three different incident energies. The average is taken over the events with b 3fm. The incident energy is indicated at the top of each figure. The extracted number is scaled by the number of nucleons in each nucleus Lower: Average nuclear density, projected on the Z axis, vs time is plotted for the same events. The contour scale is linear and arbitrarily normalized.

In Fig.4 the time evolutions of the nuclear density and momentum distributions for a central event at 35A MeV are shown for expanded scales in space and time. Two nuclei merge together at t=50fm/c as seen in the left column. At this time, however, the momentum distribution in the middle column still shows an ellipsoid stretched in the beam direction. The average dissipated energy is 3.4A MeV, which is about a half of the maximum dissipated energy reached at $t \geq$ 100fm/c. The momentum distribution becomes closer to a spherical shape at t = 80fm/c, but the projectile still has about 20% of the initial kinetic energy on the beam direction. At this time most of the projectile wave packets are passing though the target nuclei and the entire system is ready to break into small pieces. In the right column phase space distributions are shown. One can clearly see that the projectile wave packets are still moving along the beam axis at the time of the full overlap and continuing to move to the same direction. A two peak structure in the phase space at 80fm/c indicates that the energy dissipation is incomplete and the system has no chance to bounce back to a

single source. The essential feature of the above observations remain the same for the reactions at higher incident energies.

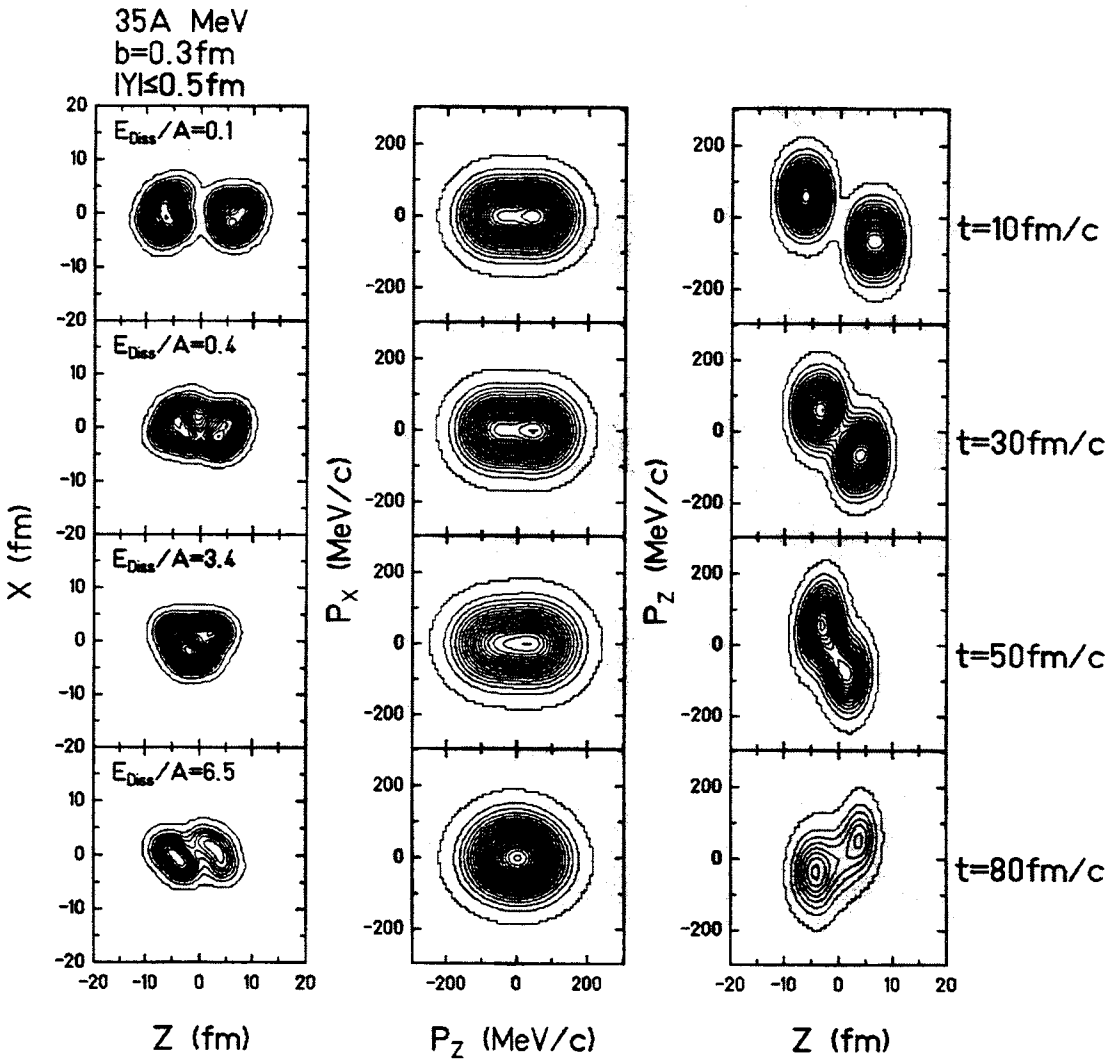

Figure 4. Left: Time evolution of the nuclear density distribution in the X-Z plane for Gaussian wave packets near the reaction plane (-0.5fm ≤Y ≤ 0.5fm) is plotted for a central event with b=0.3fm at 35A MeV. The plotted time is indicated on the right. The average dissipated energy at the given time is also given in each figure. Middel: Time evolution of the momentum distribution in the X-Z plane for the Gaussian wave packets of the same set plotted on the left. Right: Time evolution of the phase space distribution projected in the PZ-Z plane for all of the Gaussian wave packets. All contour scales are linear and arbitrarily normalized.

In order to further study the dynamics of multifragmentation, the maximum nuclear density of the largest fragment and radial flow momenta are investigated as a function of time for central events. The extracted maximum densities are normalized by the normal nuclear density ρ_o = 0.163 fm^{-3}. The radial flow momenta are calculated in the projectile rest frame in order to isolate the radial flow from the other kinetic energy contributions. The radial flow is studied in two directions; the perpendicular direction (Y direction) to the reaction plane and the parallel direction (Z direction) to the beam axis. Radial flow momenta, F_Y and F_Z, are defined as;

$$F_Y = \{1/A_p\} \sum_{i=1}^{A_p} \text{sign}(Y)\, P_Y$$

$$F_Z = \{1/A_p\} \sum_{i=1}^{A_p} \text{sign}(Z)\, P_Z$$

A_p is the mass number of the projectile and the summation is taken over all the wave packets in the projectile. F_Y and F_Z are evaluated by averaging over all events in a given impact parameter range. A positive (or negative) value of the flow momentum indicates that, on average, the wave packet is moving outward (or inward) and therefore the projectile is expanding (shrinking). The calculated results are shown in Fig.5 for the events with $b \leq 3$fm.The time evolution of the maximum nuclear density of the largest fragment, shown at the upper row, is very similar at all incident energies. The density reaches a peak at an early stage, when the two nuclei are overlapped and then returns to a density close to the normal nuclear density. In order to study the multifragmentation process in detail, three phases are introduced in the reaction time, shown by the vertical dotted lines in the figures. Phase I is the time period from the time when two nuclei touch each other to the time when the two nuclei are fully overlapped. Phase II is the time period at the time of the overlap to the time when the maximum density returns to the normal nuclear density and Phase III is attributed to the time period after that. The density reaches the maximum of about $1.6\rho_o$ at t = 50fm/c at 35A MeV and the maximum increases only slightly when the incident energy increases. The maximum nuclear density in Phase III is determined by the density in fragments. At 35A MeV the density reaches the lowest value of $0.9\rho_o$ at t = 230fm/c (which is not shown) and gradually return to the normal density. At 79A MeV, the density reaches the lowest value of $0.8\rho_o$ at t = 130-140fm/c and returns to $0.9\rho_o$ at t = 300fm/c.

In the lower row of Fig.5, the time evolution of the radial flow momentum of the projectile is shown. At 35A MeV, the radial flow momentum of the projectile stays zero in Phase I and starts to increase at the end of Phase I, just before the two nuclei are fully overlapped. The increase rate of the radial flow in the Y and Z is very similar, suggesting that the projectile expands thermally. In Phase III the projectile expands more or less at a constant velocity, although the radial flow momentum F_Z in the beam direction is twice larger than that of the Y. This difference suggests that the projectile is slightly stretched in the beam direction during the semi transparent process. At 49A MeV the situation is slightly different from that at 35A MeV. At the end of Phase I the radial flow momentum F_Y starts to become positive, whereas F_Z first becomes negative. This indicates that the projectile starts to expand in the Y direction, whereas the projectile is compressed in the beamdirection at this time. This compression results in the faster expansion in the beam direction in Phase II and the slightly larger values

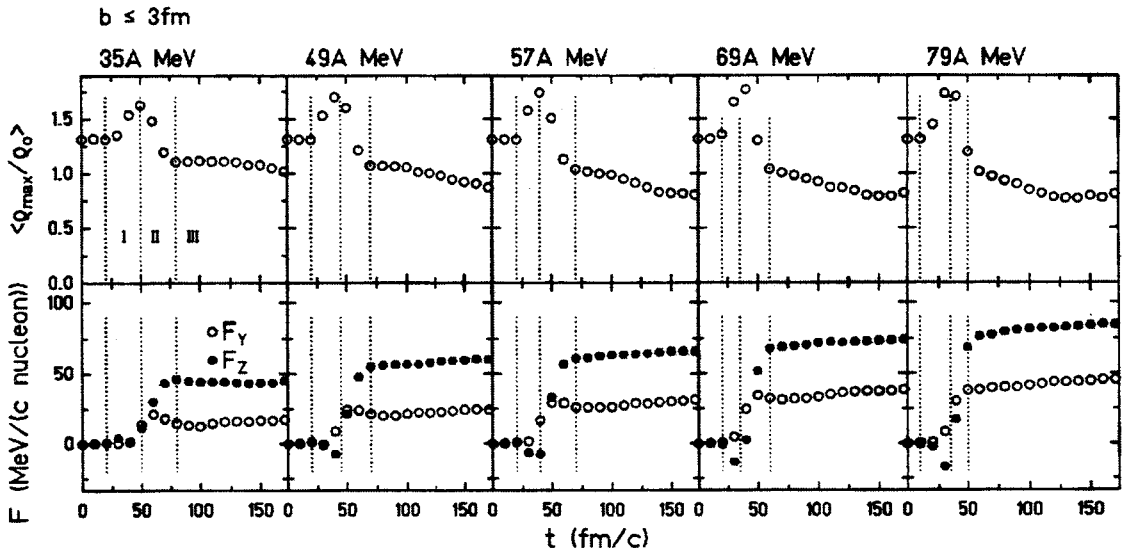

Figure 5.Average maximum nucelar density (upper) and the radial flow momenta in the projectile (lower) are plotted as a function of the reaction time for central events (b ≤ 3fm) at all incident energies. The incident energy is indicated on the top of each column. Vertical dashed lines in each figure indicate three different phases in time, discussed in the text. In the lower figures dots indicates the radial flow momentum F_Z in the beam direction and circles indicates F_Y in the perpendicular direction to the reaction plane.

of the resultant radial flow momenta in Phase III, compared to those at 35A MeV. The increase rate of F_Y is similar to that at 35A MeV, suggesting the the expansion in the Y direction is thermal. In Phase III, the difference between F_Z and F_Y is similar to that at 35A MeV, indicating that a similar stretch of theprojectile occurs in the beam direction during the semi transparent process. At higher incident energies, the characteristic features of the expansion process are essentially the same as that at 49A MeV. The negative value of F_Z increases gradually when the incident energy increases, indicating that more compression occurs at the higher incident energies. As a result the expansion rate increases in Phase II and the resultant F_Z F_Y and F_Z also increases in Phase III. The difference of the radial flow momenta F_Y and F_Z stays more or less constant. The compression mechanism at higher incident energies can be qualitatively understood as follows.The nuclear density during the collisions is governed by two factors. One is the mean field and the other is the two nucleon collision process. When the projectile nucleons enter into the target mean field in Phase I, they are accelerated by the attractive mean field and the projectile tends to be stretched in the beam direction. At the same time, on the other hand, two nucleon collisions occur and the projectile nucleons are slowed down. At 35A MeV, these two processes are more or less balanced and F_Z stays zero. At 49A MeV and higher energies, the mean field acceleration becomes slightly smaller because the interaction time is shorter. On the other hand the deceleration process by the two nucleon collisions becomes more significant because the number of the Pauli-allowed collisions increases and the momentum transfer in a collision also increases. As a result the density

compression occurs in the beam direction at the higher energies.

In summary AMD-V predicts multifragmentation at all incident energies studied here, in agreement with the experimental observations. A semi transparency is predicted at all incident energies even for central collisions. About 75% of the projectile nucleons pass through the target nucleus and appear in the forward direction with a significant energy dissipation. The dynamics of the multifragmentation process is also studied in detail. The study suggests that, at 35A MeV, thermal expansion and the semi transparency are the dominant mechanisms for the multifragmentation process, whereas, at 49A MeV and the higher incident energies, the nuclear compression occurs and plays animportant role in the multifragmentation process in addition to the thermal expansion and the semi transparency.

Reference

1. A.Ono and H.Horiuchi, Phys.Rev. **C53**, 2958 (1996).